IAHR AIRH
Taylor & Francis
Taylor & Francis Group

Journal of Hydraulic Research Vol. 53, No. 3 (2015), pp. 291–301
http://dx.doi.org/10.1080/00221686.2015.1021717

Case study

Field measurements of unsteady turbulence in a tidal bore: the Garonne river in October 2013

David Reungoat, Lecturer, *University of Bordeaux, I2M - Laboratoire TREFLE, Pessac, France*
Email: reungoat@enscbp.fr

Hubert Chanson (IAHR Member), Professor, *School of Civil Engineering, The University of Queensland, Brisbane, Australia*
Email: h.chanson@uq.edu.au (Corresponding Author)

Claire E. Keevil, PhD Research student, *University of Hull, Department of Geography, Environment and Earth Sciences, Hull HU6 7RX, United Kingdom*
Email: c.keevil@hull.ac.uk

ABSTRACT
A tidal bore is an unsteady rapidly-varied open channel flow generated by the swift advance of the early flood tide in a funnel-shaped river estuary when the tidal range exceeds 4.5 to 6 m. This contribution presents a detailed field investigation conducted on the tidal bore of the Garonne River (France). The bore was undular and the bore's leading edge was followed by well-defined secondary waves, or whelps. The instantaneous ADV velocity data indicated large and rapid fluctuations of all velocity components during the tidal bore. Large Reynolds shear stresses were observed during and after the tidal bore passage. The investigation characterized some unusual transient turbulence caused by the bore propagation in a large river system, and the results suggested the advection of large-scale eddies in the wake of the bore front. The present study highlighted the need for detailed field measurements with fine temporal resolution, to characterize the highly unsteady rapidly-varied nature of tidal bore flows.

Keywords: Acoustic Doppler velocimetry; field measurements; Garonne River; tidal bore; large-scale structures; turbulence

1 Introduction

A tidal bore may form at the leading edge of the flood tide in an estuary, when the tidal range exceeds 4.5–6 m and the channel bathymetry amplifies the flood tidal wave (Chanson, 2011; Tricker, 1965). The bore is a rapidly-varied, unsteady free-surface flow characterized by a discontinuity of the water depth, and velocity and pressure fields (Liggett, 1994; Lighthill, 1978). In an estuary, the occurrence of a tidal bore relies upon a delicate balance between the tidal amplitude, the freshwater discharge, and the river mouth and channel bathymetry. This balance may be disturbed by changes in boundary conditions and freshwater runoff; for example, a number of man-made interventions have led to the modification and sometimes disappearance of tidal bores in France, Canada, Mexico (Chanson, 2011). Bores, or positive surges, may also be observed in canals and flumes (Benet & Cunge, 1971; Treske, 1994). A related process is a tsunami wave propagating upriver led by a positive surge (Tanaka et al., 2012). Such tsunami-induced bores may propagate far upstream, as seen in Japan in 1983, 2001, 2003 and 2011, and during the 26 December 2004 tsunami disaster in the Indian Ocean.

During the early flood tide, the steepening of the free-surface and formation of the tidal bore may be predicted using the shallow-water equations (Liggett, 1994; Stoker, 1957). After inception, the front of the bore can be analysed as a hydraulic jump in translation (Chanson, 2012; Lighthill, 1978). Neglecting the boundary friction, the continuity and momentum principles provide an expression of the ratio of conjugate cross-section areas A_2/A_1 as a function of the tidal bore Froude number F_1:

$$\frac{A_2}{A_1} = \frac{1}{2}\frac{\sqrt{\left(2-\frac{B'}{B}\right)^2 + 8\frac{B'/B}{B_1/B}\mathsf{F}_1^2} - \left(2-\frac{B'}{B}\right)}{\frac{B'}{B}} \quad (1)$$

where A_1 is the initial flow cross-section area, A_2 is the conjugate flow cross-section area immediately after the bore passage,

Received 18 September 2014; accepted 17 February 2015/Open for discussion until 31 December 2015.

ISSN 0022-1686 print/ISSN 1814-2079 online
http://www.tandfonline.com

Table 1 Details of field measurements of tidal bores

Reference (1)	River (2)	Date (3)	Bore type (4)	F_1 (5)	U m s^{-1} (6)	V_1 m s^{-1} (7)	d_1 m (8)	A_1 m^2 (9)	B_1 m (10)	d_2-d_1 m (11)	B_2/B_1 (12)	B/B_1 (13)	B'/B_1 (14)	A_2/A_1 (15)	a_w/L_w (16)	$L_w/(A_1/B_1)$ (17)	T_w (s) (18)
Wolanski et al. (2004)	Daly River	2/07/03	Undular	1.04	4.70	0.15	1.50	289.3	129.2	0.28	1.013	1.007	1.001	1.13	0.0009	19.89	9.48
Simpson et al. (2004)	Dee River	6/09/03	Breaking	1.79	4.1	0.15	0.72	39.3	68.3	0.45	1.066	1.030	1.085	1.80	–	–	–
Chanson et al. (2011)	Garonne River	10/09/10	Undular	1.30	4.49	0.33	1.77	105.7	75.4	0.50	1.083	1.042	1.018	1.37	0.061	3.97	1.24
		11/09/10	Undular	1.20	4.20	0.30	1.81	108.8	75.8	0.46	1.076	1.032	1.021	1.33	0.047	3.75	1.28
Mouazé et al. (2010)	Sélune River	24/09/10	Breaking	2.35	2.00	0.86	0.38	5.25	34.7	0.34	3.37	2.33	1.92	6.19	–	–	–
		25/09/10	Breaking	2.48	1.96	0.59	0.33	3.56	33.2	0.41	3.53	2.33	1.98	9.79	–	–	–
Furgerot et al. (2013)	Sée River	7/05/12	Undular	1.39	3.2	0.4	0.9	14.82	21.7	0.56	1.101	1.060	1.046	1.87	0.014	6.26	1.34
Reungoat et al. (2014a)	Garonne River	7/06/12	Undular (very flat)	***1.02***	***3.85***	0.68	2.72	158.9	79.0	0.45	1.067	1.033	1.043	1.233	–	–	–
		7/06/12	Undular	1.19	4.58	0.59	2.65	152.3	78.7	0.52	1.071	1.032	1.040	1.278	–	–	–
Present study	Garonne River	19/10/13	Undular	1.27	4.32	0.26	2.05	85.6	65.0	0.30	1.031	1.013	1.011	1.231	0.027	2.90	0.96

Notes: A_1: channel cross-section area immediately prior to the bore passage; a_w: wave amplitude of first undulation; B_1: free-surface width immediately prior to the bore passage; d_1: water depth next to ADV immediately prior to the bore passage; F_1: tidal bore Froude number (Eq. (4)); L_w: wave length of first undulation; T_w: period of first undulation; U: tidal bore celerity positive upstream on the channel centreline; V_1: downstream surface velocity on the channel centreline immediately prior to the bore passage; (–): data not available; ***Bold italic data***: incomplete data.

Figure 1 Tidal bore of the Garonne River (France), looking downstream. (a) Bore entering the Arcins Channel on 19 October 2013 – Arcins Island is on the left of the photograph. Note the Airbus barge in the background travelling upstream behind the tidal bore. (b) Bore at Podensac on 24 August 2013, 26 km upstream of Arcins

B and B' are characteristic channel widths:

$$B = \frac{A_2 - A_1}{d_2 - d_1} \tag{2}$$

$$B' = \frac{\int_{A_1}^{A_2} \int \rho\, g\, (d_2 - z)\, \mathrm{d}A}{\frac{1}{2}\rho\, g\, (d_2 - d_1)^2} \tag{3}$$

z is the vertical distance from the bed, d_1 and d_2 are respectively the initial and new flow depths, and the Froude number F_1 is defined as:

$$\mathsf{F}_1 = \frac{V_1 + U}{\sqrt{g \frac{A_1}{B_1}}} \tag{4}$$

V_1 is the initial river flow velocity positive downstream, U is the bore celerity positive upstream, g is the gravity acceleration, B_1 is the initial free-surface width (Chanson, 2012). For a bore in a rectangular prismatic channel, Eq. (1) yields to the classical Bélanger equation (Bélanger, 1841; Liggett, 1994).

In the present study, new field measurements were conducted during the tidal bore of the Garonne River (France) on 19 October 2013. The free-surface properties were compared with the re-analysis of previous field data sets (Table 1). The instantaneous velocity measurements were performed continuously at high frequency (200 Hz) prior to, during and after the tidal bore. It is the aim of this contribution to simultaneously characterize the unsteady water elevation and velocity field, including the Reynolds stresses.

2 Site study and instrumentation

The Garonne River, France, experiences a tidal bore in the region between Bordeaux and for the next 50 km upstream (Fig. 1). Field measurements were conducted in the Arcins Channel of the Garonne River, between Arcins Island and the eastern bank, about 6.5 km south-west of the centre of the City of Bordeaux (Fig. 2). The Arcins channel is 1.8 km long, 70 m wide and about 1.1 to 2.5 m deep at low tide. Figure 1a shows the tidal bore entering the Arcins Channel and Figure 2b shows a surveyed cross-section, with the vertical elevation in m NGF IGN 1969, where NGF IGN stands for Nivellement Général de la France by the Institut Géographique National. The field study was conducted under spring tide conditions in the afternoon of 19 October 2013, at the site used by Chanson, Reungoat, Simon, & Lubin (2011) and Reungoat, Chanson, & Caplain (2014a). The tidal range was 6.09 m and the tidal cycles presented some diurnal inequality on 19 October 2013. The measurements commenced during the ebb tide prior to the passage of the bore and were conducted continuously for a further 1.5 h after the bore. Further information on the field study and data were reported in Reungoat, Chanson, & Keevil (2014b).

The free surface elevation was measured manually using a survey staff; during the bore front passage, it was recorded using

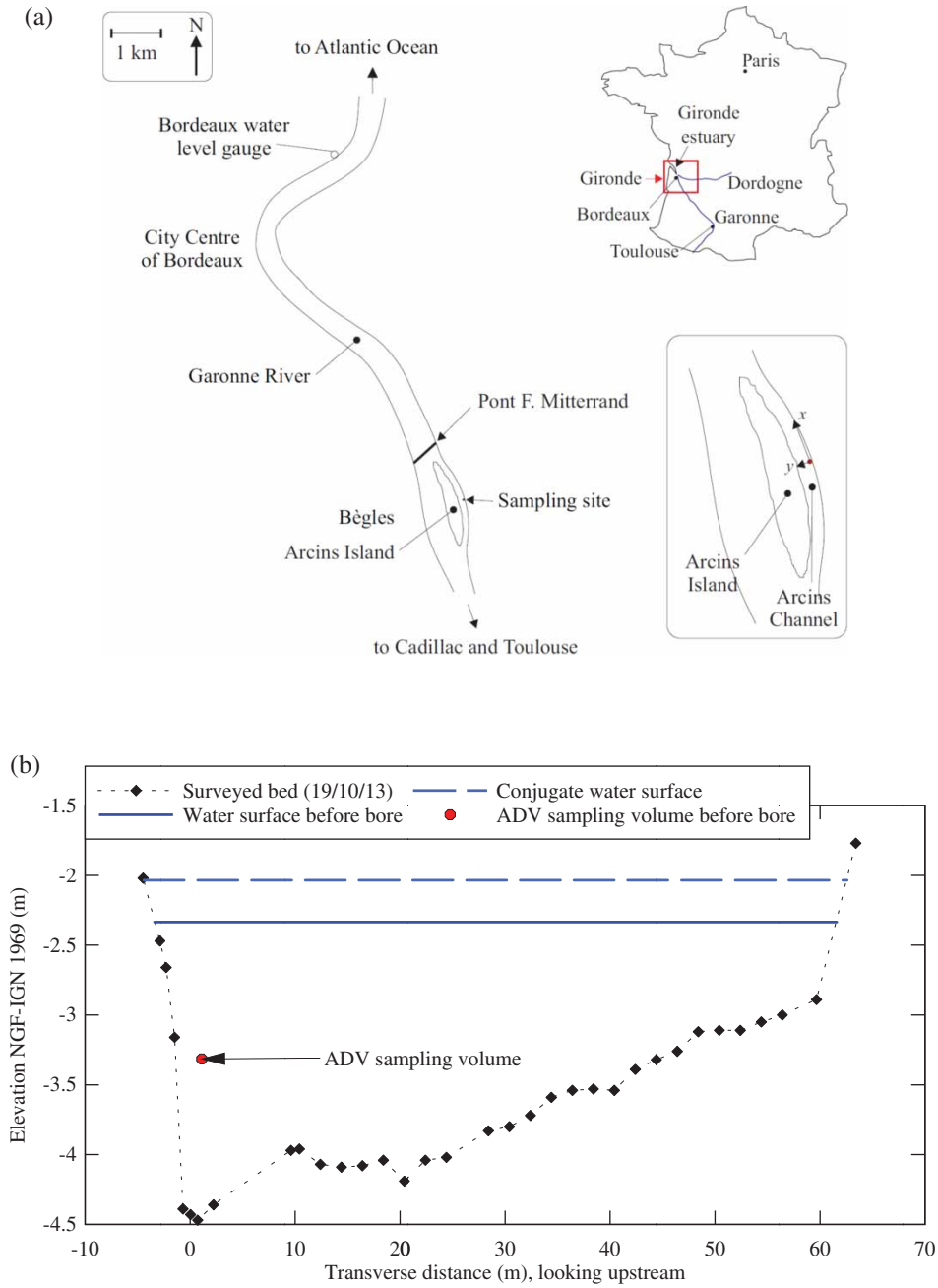

Figure 2 Sampling site. (a) Sketch of Garonne River and Arcins Island (inset: Map of France and coordinate system in the Arcins Channel). (b) Surveyed cross-section of the Arcins Channel on 19 October 2013 at the sampling site, looking upstream (i.e. South) – water levels immediately before and after bore front are shown for 19 October 2013, as well as ADV sampling volume location prior to the bore arrival

a video camera at 25 fps. The survey staff was mounted 2 m from the acoustic Doppler velocimeter (ADV), to minimize any interference with the sampling volume. The instantaneous velocity components were recorded with a Nortek ADV Vectrino+ (10 MHz, serial number VNO1356). The ADV system was equipped with a down-looking head (Field probe) equipped with four receivers. The ADV was mounted vertically 0.98 m below the surface, beneath the hull of a heavy and sturdy pontoon. Figure 2 illustrates the ADV sampling volume location in the surveyed cross-section at the end of the ebb tide. Herein, the velocity range was 2.5 m s^{-1}, and the ADV setup included a transmit length of 0.3 mm and a sampling volume of 1.5 mm height. The ADV was sampled continuously at 200 Hz. All ADV data underwent a post-processing procedure to eliminate any erroneous or corrupted data, using the software WinADV version 2.028. The post-processing included the removal of communication errors, the removal of average signal to noise ratio (SNR) data less than 5 dB, the removal of average correlation values less than 60% following McLelland & Nicholas (2000) and despiking using the phase-space thresholding technique developed by Goring & Nikora (2002). The percentage of good samples was superior to 82% for the entire data set.

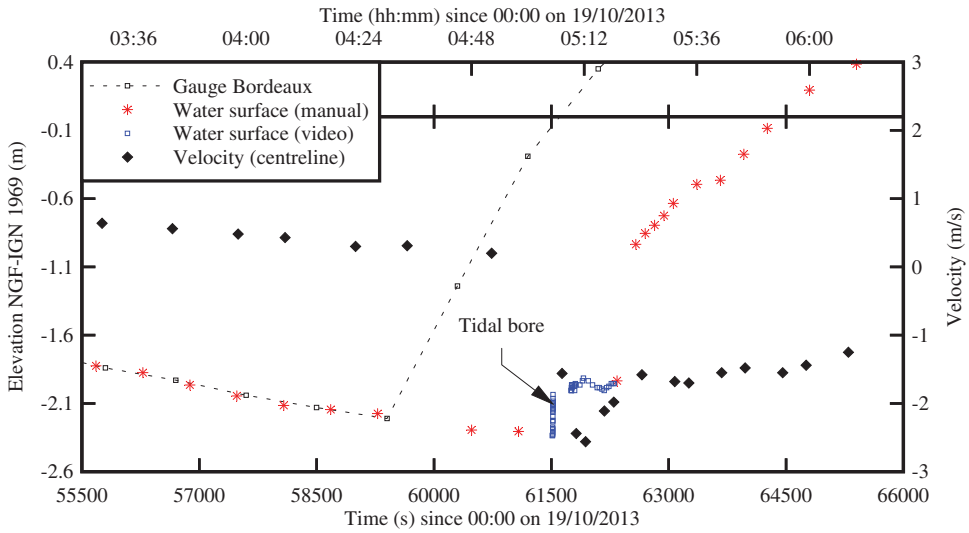

Figure 3 Time variations of the water surface elevation next to the ADV unit and free-surface velocity at the channel centre – comparison with the measured water elevations at Bordeaux (44°52′N, 0°33′W), 10 km downstream of the Arcins Channel (Data: Vigicrue, Ministère de l'Environnement et du Développement Durable)

3 Flow patterns and bore properties

The tidal bore formed at the northern end of the Arcins channel, extending across the entire width (Fig. 1a). During its upstream propagation, the bore was undular, including at the sampling location, but changed shape rapidly in response to local channel bathymetry. The bore front was well marked (e.g. by the surfers seen in Fig. 1a) and it was followed by a series of undulations (or whelps) lasting for a few minutes, with a wave period of about 1 s. The free-surface elevation rose very rapidly by 0.3 m in the first 10 – 15 s and by further 1.1 m during the next 60 s (Fig. 3). Figure 3 shows the water elevation data at Arcins and Bordeaux, the latter gauge being located 10 km downstream of the Arcins Channel and shown in Fig. 2a. The passage of the tidal bore on 19 October 2013 is clearly seen in Fig. 3 and the data are further compared with surface velocity measurements in the centre of the Arcins Channel.

The tidal bore front correspondedto a marked rise in free-surface elevation. The Froude number was calculated based upon the surveyed channel cross-section and field observations yielding $\mathsf{F}_1 = 1.27$ (Table 1), which was consistent with the undular nature of the bore. The present observations are reported in Fig. 4 in terms of the ratio of conjugate cross-sectional areas A_2/A_1 as a function of the Froude number. The current data (red star symbol) are compared with the momentum principle solution (Eq. (1)) (open circles) and previous field data (Table 1) (Fig. 4). For comparison, the classical Bélanger equation, developed for a smooth rectangular channel, is also shown:

$$\frac{d_2}{d_1} = \frac{1}{2}\left(\sqrt{1 + 8\,\mathsf{F}_1^2} - 1\right) \quad (5)$$

Figure 4 indicates a good agreement between Eq. (1) and tidal bore field data, demonstrating the limitations of the Bélanger

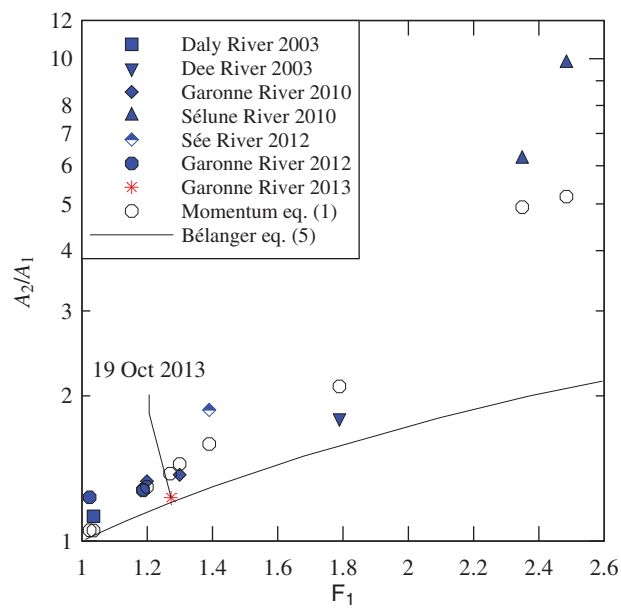

Figure 4 Relationship between the conjugate cross-sectional area ratio A_2/A_1 and Froude number F_1 for tidal bore field observations – comparison with the momentum principle (Eq. (1)) and the classical Bélanger equation (Eq. (5))

equation (Eq. (1)) in natural channels. Our result, although close to the Bélanger equation, is similar to all the results from previous studies by considering the measurement accuracy. The full data sets are reported in a tabular format in Table 1.

The passage of theundular bore was followed by a rapid rise in water elevation ($t = 61512$ s in Fig. 3) and some marked secondary wave motion behind the front. A key feature was the smooth bore front followed by free-surface undulations, a feature of undular bores previously documented in the field (Chanson et al., 2011; Wolanski, Williams, Spagnol, & Chanson, 2004). The dimensionless undulation characteristics are shown in Fig. 5: i.e., the wave length and wave steepness.

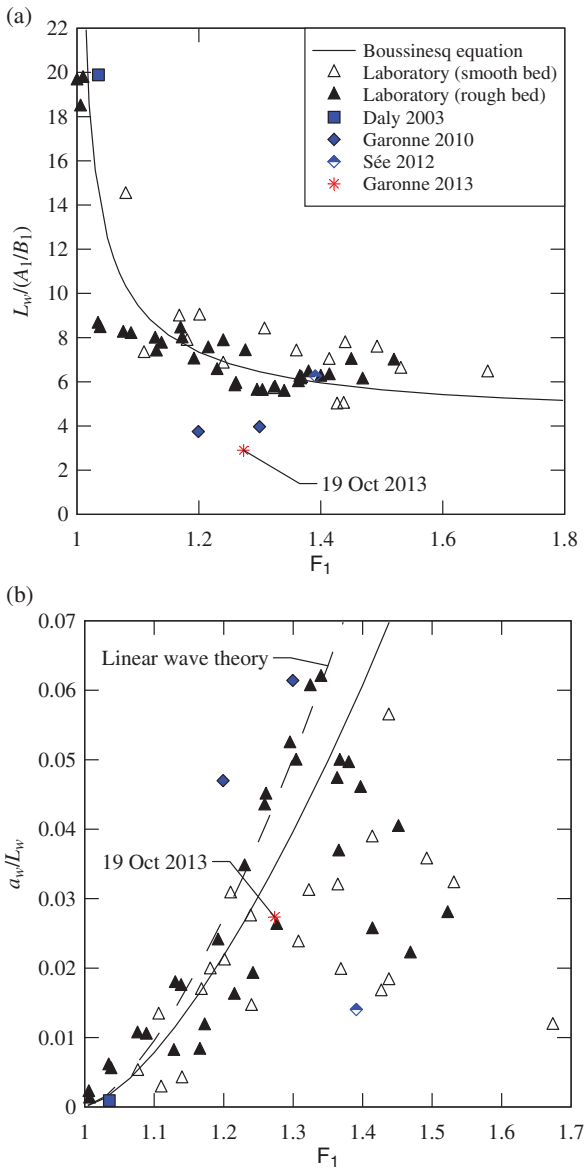

Figure 5 Free-surface undulation properties in tidal bores – comparison with laboratory data, linear wave theory (dashed line) and Boussinesq equation solution (solid line). Same legend for both graphs. (a) Dimensionless wave length; (b) wave steepness

In Fig. 5, the present observations are compared with field and laboratory data of undular bores, as well as to analytical solutions based upon the linear wave theory and Boussinesq equations (Andersen, 1978; Lemoine, 1948). The dimensionless wave length $L_w/(A_1/B_1)$ decreased with increasing Froude number and the data were relatively close to a solution of the Boussinesq equation (Fig. 5a). The undulation wave steepness a_w/L_w increased with increasing Froude number up to $F_1 = 1.3$ (Fig. 5b). For larger Froude numbers, the wave steepness was restricted by the appearance of some breaking at the first wave crest and the data tended to decrease with increasing Froude number for $F_1 > 1.3$. In Fig. 5, the current data (red star symbol) showed comparable trends with previous observations, despite the irregular bathymetry of the natural channel.

4 Instantaneous velocity and turbulent stress data

The instantaneous velocity components were measured continuously prior to, during and after the undular tidal bore. Figure 6 shows the velocity data about the time of passage of the bore front, with the longitudinal velocity component V_x positive downstream, the transverse velocity component V_y positive towards Arcins Island, and the vertical velocity component V_z positive upwards. The water depth measurements are also included in Fig. 6.

For the last two hours of the ebb tide the current velocity dropped from $+0.6$ m s^{-1} down to $+0.1$ m s^{-1} (Fig. 3 and 6). The passage of the tidal bore ($t = 61512$ s, Fig. 6) induced a marked effect on the velocity field and water depth. The main current reversed its direction almost immediately and the mean longitudinal velocity ranged typically between -0.8 and -1.2 m s^{-1} after the bore passage, where the negative sign reflected the upriver flow direction. The bore passage induced strong mixing in the channel; although the free-surface ahead of the first wave crest appeared smooth, intense mixing was observed at the water surface next to the banks when the bore arrived. The bore passage was associated with loud crashes of waters on the pontoons, boat ramps and banks.

During the bore passage, the mean longitudinal flow deceleration was -0.18 m s^{-2}, or $-0.02 \times g$. The tidal bore front was characterized by large fluctuations of all velocity components (Fig. 6). The longitudinal velocity component fluctuated between -0.6 and -1.35 m s^{-1} after the passage of the bore, the transverse velocities ranged from -0.2 to $+0.35$ m s^{-1}, while the vertical velocity data fluctuated between -0.3 and $+0.1$ m s^{-1}. The vertical velocity data showed some oscillations with a period about 1 to 1.5 s immediately after the bore passage: i.e., $61520 < t < 61555$ s in Fig. 6. It is believed that these oscillations were closely linked with the free-surface undulations, or whelps, and their induced vertical motion. The irrotational flow theory predicts a redistribution of both longitudinal and vertical velocities between wave crests and troughs, with the same periodicity as the free-surface elevation but out of phase (Montes & Chanson, 1998; Rouse, 1938). This pattern would be consistent with the current observations and was previously documented in laboratory tidal bores (Chanson, 2010; Koch & Chanson, 2008).

The turbulent properties were estimated during the late ebb tide and early flood tide including for the tidal bore passage. Herein, the turbulent velocity fluctuation v was the deviation of the instantaneous velocity V from a 'mean' value, which was the low-pass filtered value, or variable interval time average VITA, calculated using a threshold frequency of 2 Hz (Reungoat et al., 2014b). The threshold frequency was selected between the free-surface undulation frequency ($1/T_w$) and twice the undulation frequency ($2/T_w$) based upon a sensitivity analysis, following earlier works (Chanson & Docherty, 2012; Chanson et al., 2011). Some basic turbulence characteristics are summarized in Tables 2 and 3, in terms of the dimensionless velocity

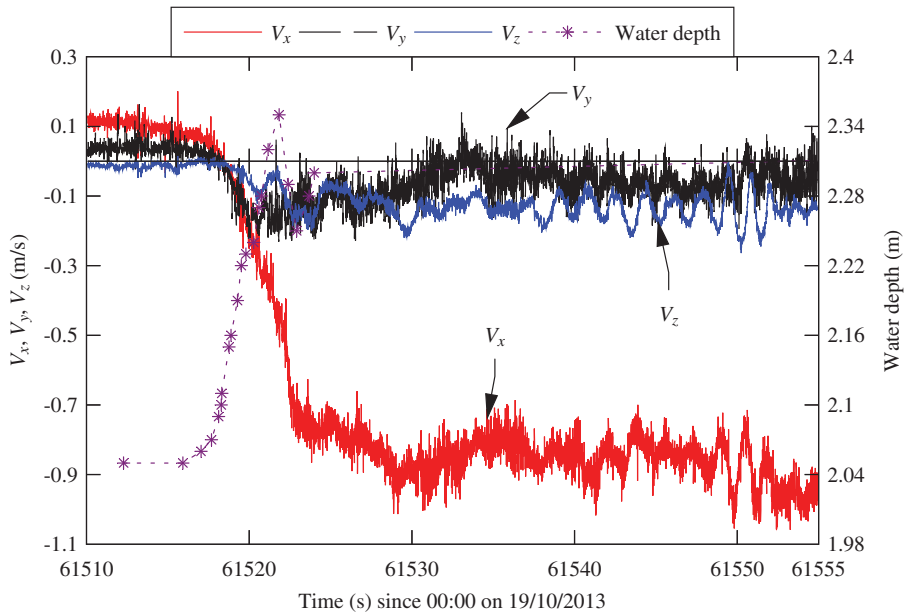

Figure 6 Instantaneous velocity components and water depth as functions of time during the tidal bore passage on 19 October 2013

Table 2 Turbulence properties before and after the tidal bore of the Garonne River on 19 October 2013

Description	Time since 19/10/13 00:00 (s)	$\overline{V_x}$ (m s^{-1})	$\frac{v_x'}{\overline{\lvert V_x \rvert}}$	$\frac{v_y'}{\overline{\lvert V_x \rvert}}$	$\frac{v_z'}{\overline{\lvert V_x \rvert}}$	$\frac{v_y'}{v_x'}$	$\frac{v_z'}{v_x'}$
(1)	(2)	(3)	(4)	(5)	(6)	(7)	(8)
End ebb tide	61292–61492	+ 0.109	0.242	0.195	0.120	0.806	0.495
Immediately prior to tidal bore	61492–61512	+ 0.100	0.191	0.149	0.091	0.779	0.475
Immediately after tidal bore	61522–61542	− 0.823	0.089	0.064	0.040	0.723	0.446
Early flood tide	62090–62290	− 0.869	0.157	0.112	0.074	0.712	0.472
Mid-flood tide (end of study)	65600–65800	− 1.162	0.066	0.042	0.025	0.639	0.384

Note: V_x: longitudinal velocity positive downstream.

fluctuations and integral time scales. Although the velocity fluctuations were larger in the late ebb tide, the dimensionless fluctuations $v_x'/|\overline{V_x}|$, $v_y'/|\overline{V_x}|$ and $v_z'/|\overline{V_x}|$ were of similar magnitude before and after the bore passage, although smaller after the bore, where v_x', v_y' and v_z' are the standard deviations of the longitudinal, transverse and vertical velocity components respectively, and $|\overline{V_x}|$ is the amplitude of the mean longitudinal velocity component. The horizontal turbulence ratio v_y'/v_x' was equal to 0.7–0.8 before and after the bore (Table 2), with values comparable to laboratory observations in straight prismatic rectangular channels ($v_y'/v_x' = 0.5$–0.7, Nezu & Nakagawa, 1993). The vertical turbulence ratio v_z'/v_x' was about 0.4–0.5 (Table 2): i.e., similar to the observations of Shiono & West (1987) and Trevethan, Chanson, & Brown (2008) in estuaries, and Nezu & Nakagawa (1993) and Xie (1998) in laboratory open channels. Note that v_z'/v_y' was approximately two-thirds, implying some turbulence anisotropy. The integral turbulent time scales of each velocity component represented a measure of the longest connection in the turbulent behaviour of that velocity component. The experimental data showed some differences between before and after the bore (Table 3). The integral time scale of the longitudinal velocity component was on average 10 times larger after than before the bore passage. Reungoat et al. (2014a) reported a similar observation, which is believed to be linked to the production and advection of large eddies behind the bore, as shown by numerical models (Furuyama & Chanson, 2010; Lubin, Chanson, & Glockner, 2010). The integral times scales in terms of the transverse and vertical velocities were of the same order of magnitude before and after the bore (Table 3).

4.1 *Turbulent Reynolds stresses*

A Reynolds stress is proportional to the cross-product of turbulent velocity fluctuation v, where v is the deviation of the instantaneous velocity V from the VITA value (see above). The method was applied to all velocity components and the turbulent Reynolds stresses were calculated from the high-pass filtered signals. Typical results are presented in Fig. 7.

The field observations showed large turbulent shear stresses, and large and rapid fluctuations in shear stresses during and after the tidal bore, for all Reynolds stress tensor components. The data indicated that the turbulent shear stresses were

Table 3 Integral turbulent time scales before and after the tidal bore on 19 October 2013

Description (1)	Time since 19/10/13 00:00 (s) (2)	$\overline{V_x}$ (m s^{-1}) (3)	T_{Vx} (s) (4)	T_{Vy} (s) (5)	T_{Vz} (s) (6)
End ebb tide	61292–61492	+ 0.109	0.973	0.384	0.375
Early flood tide	62090–62290	− 0.869	9.436	4.336	0.872
Mid-flood tide (end of study)	65600–65800	− 1.162	10.38	0.468	0.840

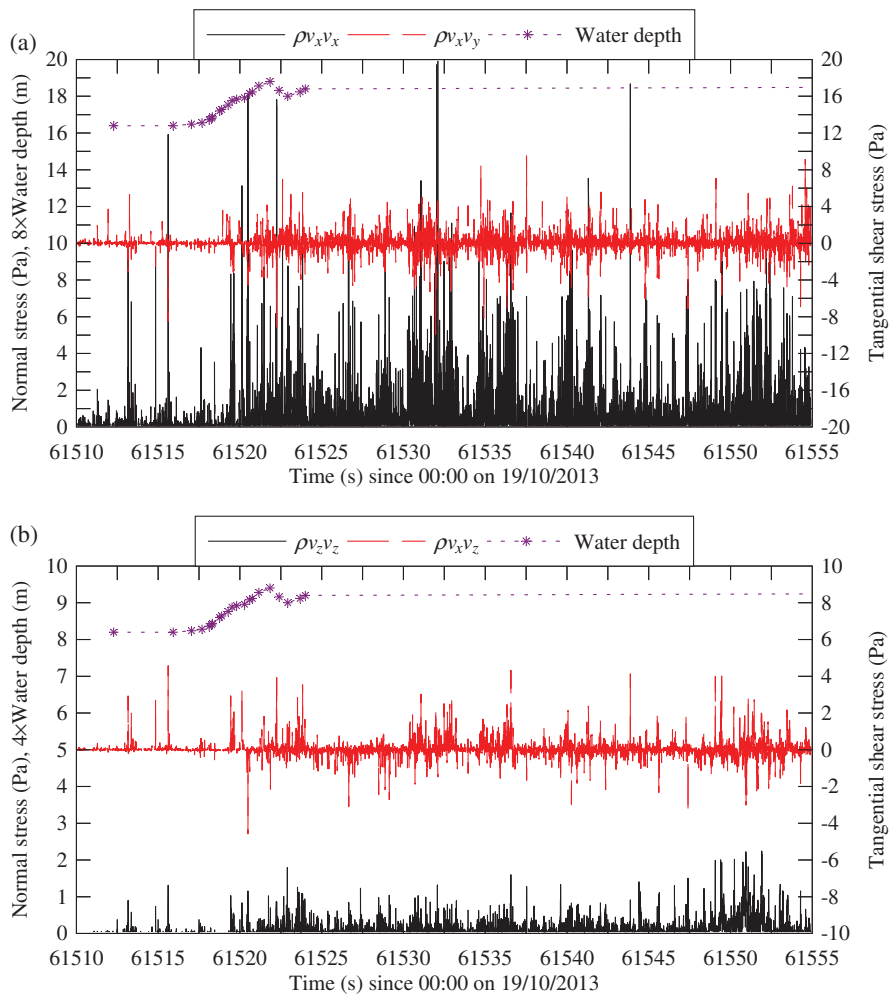

Figure 7 Instantaneous Reynolds stress tensor components and water depth as functions of time during the tidal bore passage on 19 October 2013. (a) $\rho v_x{}^2$ and $\rho v_x v_y$; (b) $\rho v_z{}^2$ and $\rho v_x v_z$

significantly larger in the wake of the tidal bore (Fig. 7). Maximum instantaneous shear stress amplitudes of up to 80 Pa were recorded during and after the bore passage. The data indicated that the tidal bore likely scoured the channel bed and advected into suspension the bed material and washload upstream, behind the bore front. This was consistent with visual observations of sediment flocs bursting at the free-surface during the early flood tide. The sediment scour and advection processes applied to a significant length of the estuarine section of the Garonne River and would mobilize an enormous amount of sediments.

5 Discussion

The field measurements demonstrated large instantaneous velocity fluctuations and turbulent stresses during the tidal bore. The instantaneous velocity fluctuations (v_x, v_y, v_z) followed relatively closely a normal distribution. The longitudinal velocity fluctuation data are plotted in Fig. 8, in the form of the probability distributions functions measured before, during and immediately after the bore passage. Data were sampled in 1 cm s^{-1} bin intervals in Fig. 8. For all velocity fluctuations, the skewness ranged between 0.11 and 0.23 prior to the tidal bore and

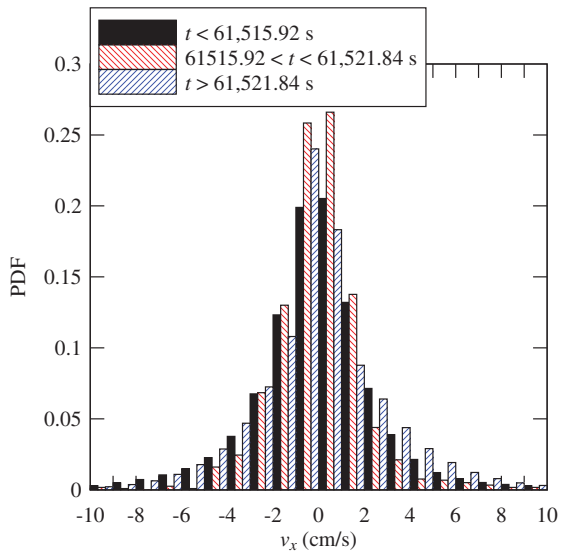

Figure 8 Probability distribution function of longitudinal velocity fluctuations v_x during the late ebb tide, bore passage and early flood tide on 19 October 2013

between 0.06 and 0.58 during the early ebb tide. Such values are comparable to skewness measurements in turbulent open channel flows and outer boundary layer flows (Nakagawa & Nezu, 1977). The excess kurtosis was between 2.5 and 4 for the v_x and v_z components, and between 0.2 and 0.3 for v_y, during both the late ebb and early flood tides.

While a turbulent flow is typically characterized by its statistical moments, a key feature is the turbulent events often associated with coherent flow structures such as eddies and bursting (Adrian & Marusic, 2012; Kline, Reynolds, Schraub, & Rundstadler, 1967). Turbulent event analyses were successfully applied to laboratory open channel flows (Nakagawa & Nezu, 1977), atmospheric boundary layer flows (Narasimha, Rudra Kumar, Trabhu, & Kailas, 2007) and even estuarine flows (Trevethan & Chanson, 2010). However they have been rarely applied to unsteady rapidly-varied estuaries. Herein, the simultaneous longitudinal and vertical velocity fluctuations, v_x and v_z respectively, were analysed into four quadrants to evaluate the contributions of the ejections and sweeps to the Reynolds stress, following Nakagawa & Nezu (1977). The four quadrants are typically called outward interaction ($v_x > 0, v_z > 0$), ejection ($v_x < 0, v_z > 0$), inward interaction ($v_x < 0, v_z < 0$) and sweep ($v_x > 0, v_z < 0$) (Nezu & Nakagawa, 1993). The Reynolds stress fluctuations were investigated by using the conditional sampling method: $|v_x v_z| > H$ where H is the hole size. The contribution to $v_x v_z$ from the hole would represent the contribution during the more quiescent periods, while the second and fourth quadrants corresponded to the burst and sweep events. The field measurement results are shown in Fig. 9. The fraction of the total time that $v_x v_z$ spent in the hole region is also included in Fig. 9. During the late ebb tide flow (Fig. 9a), the results were comparable to steady turbulent boundary layer data. For a large proportion of time, the turbulent stress $v_x v_z$ was small. The largest contribution came from the second quadrant

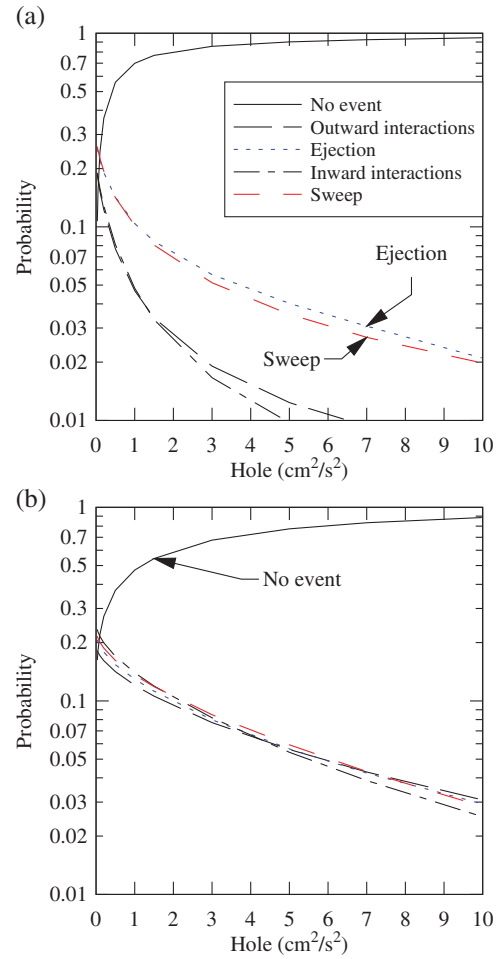

Figure 9 Fraction of time of Reynolds stress $v_x v_z$ during the late ebb tide and early flood tide on 19 October 2013 (same legend for both graphs). (a) During the late ebb tide ($58000 < t < 61515.92$ s); (b) during the early flood tide ($61521.84 < t < 63000$ s)

(burst), and the second largest contribution was the fourth quadrant (sweep). In contrast, the results during the early flood tide (Fig. 9b) indicated much larger turbulent stresses $v_x v_z$, with a lesser proportion of no-event for a given hole size. Further, the proportion of time and contribution of all four quadrants were of comparable magnitude. The findings were consistent with the observations that the early flood flow was dominated by large-scale structures generated in the wake of the bore. The interactions of these very large eddies with the free-surface were seen by all field work participants in the form of large boils and surface scars.

6 Conclusion

During a field study in the Garonne River's tidal bore, the water elevation and instantaneous velocity field was documented prior to and during the bore event with a fine temporal resolution. The tidal bore was undular and its Froude number was $\mathsf{F}_1 = 1.27$. The bore's leading edge was followed by well-defined whelps with a wave period of about 1 s, while the wave amplitude and length were comparable to theoretical estimates and earlier field

observations. The instantaneous ADV velocity data indicated large and rapid fluctuations of all velocity components. Large Reynolds shear stresses were observed during and after the tidal bore. The integral time scale and quadrant analysis results indicated some marked differences between the late ebb tide and the early flood tide flow motion immediately behind the bore. In particular the field observations suggested the upstream advection of large scale vortical structures in the wake of the bore.

The current study highlights the need for further detailed field measurements, including for the validation of any kind of modelling. A major challenge is the highly unsteady rapidly-varied nature of tidal bore flows, implying a fine temporal resolution. Altogether the field study indicated that tidal bores and positive surges in rivers and canals can generate some very intense mixing and a complex velocity field beneath the smooth free-surface. The large turbulent stresses may lead to sediment scour and suspension, impacting onto the sediment processes, water quality and ecology of the waterway. These aspects are rarely considered in numerical and laboratory models, although an accurate representation of the flow physics is critical to the advancement of science and engineering.

Acknowledgements

The authors acknowledge the assistance of Patrice Bengiati and the permission to access and use the pontoon in the Bras d'Arcins. They thank all the people who participated to the field work, without whom the study could not have been conducted. They further thank a number of scholars for their input and advice, in particular Professor Dan Parsons (University of Hull, UK), Dr Frédérique Larrarte (IFSTTAR Nantes, France), Professor Michael Bestehorn (Brandenburg University of Technology, Germany) and Professor Pierre Lubin (University of Bordeaux, France). The authors acknowledge the financial assistance of the Agence Nationale de la Recherche (Projet MASCARET 10-BLAN-0911-01).

Notation

A = cross-section area (m^2)
A_1 = inflow cross-section area (m^2)
A_2 = conjugate cross-section area (m^2)
a_w = wave amplitude (m)
B = channel width (m)
B' = characteristic channel width (m)
B_1 = inflow free-surface width (m)
d = water depth (m)
d_1 = inflow depth (m)
d_2 = conjugate flow depth (m)
F_1 = Froude number (–)
g = gravity acceleration ($m\ s^{-2}$)
H = hole size ($m^2\ s^{-2}$)
L_w = wave length (m)
T_{Vx} = integral time scale of longitudinal velocity component (s)
T_{Vy} = integral time scale of transverse velocity component (s)
T_{Vz} = integral time scale of vertical velocity component (s)
T_w = wave period (s)
t = time (s)
U = bore celerity ($m\ s^{-1}$) positive upstream
V_x = longitudinal velocity component ($m\ s^{-1}$)
V_y = tranverse velocity component ($m\ s^{-1}$)
V_z = vertical velocity component ($m\ s^{-1}$)
V_1 = inflow velocity ($m\ s^{-1}$)
v = velocity fluctuation ($m\ s^{-1}$)
v_x = longitudinal velocity fluctuation ($m\ s^{-1}$)
v_y = transverse velocity fluctuation ($m\ s^{-1}$)
v_z = vertical velocity fluctuation ($m\ s^{-1}$)
v_x' = longitudinal velocity fluctuation root mean square ($m\ s^{-1}$)
v_y' = transverse velocity fluctuation root mean square ($m\ s^{-1}$)
v_z' = vertical velocity fluctuation root mean square ($m\ s^{-1}$)
x = longitudinal coordinate positive downstream (m)
y = transverse coordinate positive towards Arcins Island (m)
z = vertical coordinate positive upstream (m)
ρ = water density ($m^3\ s^{-1}$)

References

Adrian, R. J., & Marusic, I. (2012). Coherent structures in flow over hydraulic engineering surfaces. *Journal of Hydraulic Research*, *50*, 451–464. doi:10.1080/00221686.2012.729540

Andersen, V. M. (1978). Undular hydraulic jump. *Journal of the Hydraulic Division: Proceedings of ASCE*, *104* (HY8), 1185–1188.

Bélanger, J. B. (1841). Notes sur l'hydraulique. [Notes on hydraulic engineering.] Ecole Royale des Ponts et Chaussées, Paris, France, session 1841–1842, 223 pages (in French).

Benet, F., & Cunge, J. A. (1971). Analysis of experiments on secondary undulations caused by surge waves in trapezoidal channels. *Journal of Hydraulic Research*, *9*, 11–33.

Chanson, H. (2010). Unsteady turbulence in tidal bores: Effects of bed roughness. *Journal of Waterway, Port, Coastal and Ocean Engineering - ASCE, 136*, 247–256. doi:10.1061/(ASCE)WW.1943-5460.0000048

Chanson, H. (2011). *Tidal bores, Aegir, Eagre, Mascaret, Pororoca: Theory and observations*. Singapore: World Scientific.

Chanson. H, (2012). Momentum considerations in hydraulic jumps and bores. *Journal of Irrigation and Drainage E-ASCE*, *138*, 382–385. doi:10.1061/(ASCE)IR.1943-4774.0000409

Chanson, H., & Docherty, N. J. (2012). Turbulent velocity measurements in open channel bores. *European Journal of Mechanics B-Fluid*, *32*, 52–58. doi:10.1016/j.euromechflu.2011.10.001

Chanson, H., Reungoat, D., Simon, B., & Lubin. P, (2011). High-frequency turbulence and suspended sediment concentration measurements in the Garonne River tidal bore. *Estuarine and Coastal Shelf Science*, *95*, 2–3, 298–306. doi:10.1016/j.ecss.2011.09.012

Furgerot, L., Mouazé, D., Tessier, B., Perez, L., & Haquin, S. (2013). Suspended sediment concentration in relation to the passage of a tidal bore (Sée River Estuary, Mont Saint Michel, NW France). *Proceedings of Coastal Dynamics 2013*, Arcachon, France, 24–28 June, 671–682.

Furuyama, S., & Chanson, H. (2010). A numerical solution of a tidal bore flow. *Coastal Engineering Journal*, *52*, 215–234. doi:10.1142/S057856341000218X

Goring, D. G., & Nikora, V. I. (2002). Despiking acoustic Doppler velocimeter data. *Journal of Hydraulic Engineering – ASCE*, *128*, 117–126. doi:10.1061/(ASCE)0733-9429(2002)128:1(117)

Kline, S. J., Reynolds, W. C., Schraub, F. A., & Rundstadler, P. W. (1967). The structure of turbulent boundary layers. *Journal of Fluid Mechanics*, *30*, 741–773.

Koch, C., & Chanson, H. (2008). Turbulent mixing beneath an undular bore front. *Journal of Coastal Research*, *24*, 999–1007. doi:10.2112/06-0688.1

Lemoine, R. (1948). Sur les Ondes Positives de Translation dans les Canaux et sur le Ressaut Ondulé de Faible Amplitude. [On the positive surges in channels and on the undular jumps of low wave height.] *Journal La Houille Blanche*, 183–185.

Liggett, J. A. (1994). *Fluid mechanics*. New York: McGraw-Hill.

Lighthill, J. (1978). *Waves in fluids*. Cambridge: Cambridge University Press.

Lubin, P., Chanson, H., & Glockner, S. (2010). Large eddy simulation of turbulence generated by a weak breaking tidal bore. *Environmental Fluid Mechanics*, *10*, 587–602. doi:10.1007/s10652-009-9165-0

McLelland, S. J., & Nicholas, A. P. (2000). A new method for evaluating errors in high-frequency ADV measurements. *Hydrological Processess*, *14*, 351–366. doi:10.1002/(SICI)1099-1085(20000215)14:2 < 351::AID-HYP963 > 3.0.CO;2-K

Montes, J. S., & Chanson, H. (1998). Characteristics of undular hydraulic jumps. Results and calculations. *Journal of Hydraulic Engineering, ASCE*, *124*, 192–205.

Mouazé, D., Chanson, H., & Simon, B. (2010). *Field measurements in the tidal bore of the Sélune River in the bay of Mont Saint Michel (September 2010)*. Hydraulic Model Report No. CH81/10, School of Civil Engineering, The University of Queensland. Brisbane, Australia.

Nakagawa, H., & Nezu, I. (1977). Prediction of the contribution of the Reynolds stress from bursting events in open-channel flows. *Journal of Fluid Mechanics*, *80*, 99–128.

Narasimha, R., Rudra Kumar, S., Prabhu, A., & Kailas, S. V. (2007). Turbulent flux events in a nearly neutral atmospheric boundary layer. *Philosophical Transactions of the Royal Society A*, *365*, 841–858. doi:10.1098/rsta.2006.1949

Nezu, I., & Nakagawa, H. (1993). Turbulence in open-channel flows. IAHR Monograph, IAHR Fluid Mechanics Section. Rotterdam, the Netherlands: Balkema, 281 pages.

Reungoat, D., Chanson, H., & Caplain, B. (2014a). Sediment processes and flow reversal in the undular tidal bore of the Garonne River (France). *Environmental Fluid Mechanics*, *14*, 591–616. doi:10.1007/s10652-013-9319-y

Reungoat, D., Chanson, H., & Keevil, C. (2014b). *Turbulence, sedimentary processes and tidal bore collision in the Arcins Channel, Garonne River (October 2013)*. Hydraulic Model Report No. CH94/14, School of Civil Engineering, the University of Queensland, Brisbane, Australia.

Rouse, H. (1938). *Fluid mechanics for hydraulic engineers*. New York: McGraw-Hill.

Shiono, K., & West, J. R. (1987). Turbulent perturbations of velocity in the Conwy Estuary. *Estuarine Coastal and Shelf Science*, *25*, 533–553.

Simpson, J. H., Fisher, N. R., & Wiles, P. (2004). Reynolds stress and TKE production in an estuary with a tidal bore. *Estuarine Coastal and Shelf Science*, *60*, 619–627. doi:10.1016/j.ecss.2004.03.006

Stoker, J. J. (1957). *Water waves. The mathematical theory with applications*. New York: Interscience Publishers.

Tanaka, H., Nguyen, X. T., Umeda, M., Hirao, R., Pradjoko, E., Mano, A., & Udo, K. (2012). Coastal and estuarine morphology changes induced by the 2011 Great East Japan earthquake tsunami. *Coastal Engineering Journal*, *54* (1), paper 1250010. doi:10.1142/S0578563412500106

Treske, A. (1994). Undular bores (Favre-waves) in open channels - experimental studies. *Journal of Hydraulic Research*, *32*, 355–370.

Trevethan, M., & Chanson, H. (2010). Turbulence and turbulent flux events in a small estuary. *Environmental Fluid Mechanics*, *10*, 345–368. doi:10.1007/s10652-009-9134-7

Trevethan, M., Chanson, H., & Brown, R. (2008). Turbulent measurements in a small subtropical estuary with semi-diurnal tides. *Journal of Hydraulic Engineering – ASCE*, *134*, 1665–1670. doi:10.1061/(ASCE)0733-9429(2008)134:11(1665)

Tricker, R. A. R. (1965). *Bores, breakers, waves and wakes*. New York: American Elsevier.

Wolanski, E., Williams, D., Spagnol, S., & Chanson, H. (2004). Undular tidal bore dynamics in the Daly Estuary, northern Australia. *Estuarine Coastal and Shelf Science*, *60*(4), 629–636.

Xie, Q. (1998). *Turbulent flows in non-uniform open channels: Experimental measurements and numerical modelling (PhD thesis)*. Department of Civil Engineering, University of Queensland, Brisbane, Australia.